Two [1,2,4-(Me₃C)₃C₅H₂]₂CeH Molecules are Involved in Hydrogenation of Pyridine to Piperidine as Shown by Experiments and Computations

Lionel Perrin,*[†,‡] Evan L. Werkema,[§] Odile Eisenstein,*[⊥] and Richard A. Andersen*[§]

[†]Université de Toulouse, INSA, UPS, LPCNO, 135 avenue de Rangueil, F-31077 Toulouse, France, and CNRS, F-31077 Toulouse, France

[§]Department of Chemistry, University of California, Berkeley, California 94720-1460, United States

[⊥]Institut Charles Gerhardt, CNRS UMR 5253, Université Montpellier 2, Place E. Bataillon, F-34095 Montpellier, France
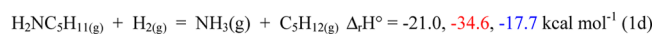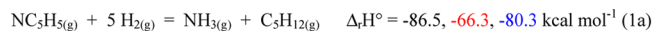
S *Supporting Information*

ABSTRACT: Hydrogenation of pyridine to piperidine catalyzed by [1,2,4-(Me₃C)₃C₅H₂]₂CeH, abbreviated as Cp′₂CeH or [Ce]′-H, is reported. The reaction proceeds from Cp′₂Ce(2-pyridyl), isolated from the reaction of pyridine with Cp′₂CeH, to Cp′₂Ce(4,5,6-trihydropyridyl), and then to Cp′₂Ce(piperidyl). The cycle is completed by the addition of pyridine, which generates Cp′₂Ce(2-pyridyl) and piperidine. The net reaction depends on the partial pressure of H₂ and temperature. The dependence of the rate on the H₂ pressure is associated with the formation of Cp′₂CeH, which increases the rate of the first and/or second additions of H₂ but does not influence the rate of the third addition. Density functional theory calculations of several possible pathways are consistent with three steps, each of which are composed of two elementary reactions, (i) heterolytic activation of H₂ with a reasonably high energy, $\Delta G^{\ddagger} = 20.5$ kcal mol⁻¹, on Cp′₂Ce(2-pyridyl), leading to Cp′₂CeH(6-hydropyridyl), followed by an intramolecular hydride transfer with a lower activation energy, (ii) intermolecular addition of Cp′₂CeH to the C⁴═C⁵ bond, followed by hydrogenolysis, giving Cp′₂Ce(4,5,6-trihydropyridyl) and regenerating Cp′₂CeH, and (iii) a similar hydrogenation/hydrogenolysis sequence, yielding Cp′₂Ce(piperidyl). The calculations reveal that step ii can only occur in the presence of Cp′₂CeH and that alternative intramolecular steps have considerably higher activation energies. The key point that emerges from these experimental and computational studies is that step ii involves two Cp′₂Ce fragments, one to bind the 6-hydropyridyl ligand and the other to add to the C⁴═C⁵ double bond. In the presence of H₂, this second step is intermolecular and catalytic. The cycle is completed by reaction with pyridine to yield Cp′₂Ce(2-pyridyl) and piperidine. The structures of Cp′₂CeX, where X = 2-pyridyl, 4,5,6-trihydropyridyl, and piperidyl, are fluxional, as shown by variable-temperature ¹H NMR spectroscopy.
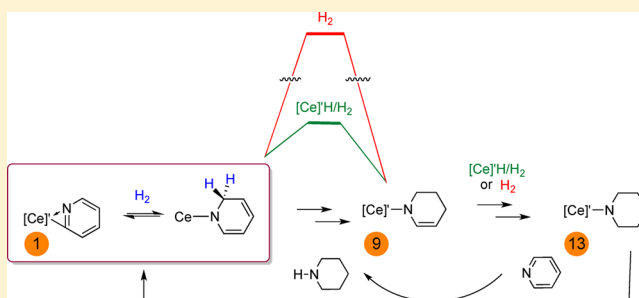
INTRODUCTION

The removal of heterocyclic amines from petroleum feedstocks is an important industrial process because these compounds form nitrogen oxides when the hydrocarbons are combusted. Removing these sources of nitrogen oxides before combustion is therefore a crucial step in eliminating these potential atmospheric contaminants. A large research effort has been expended on the removal of nitrogen-containing molecules by hydrogenation, a process referred to as hydrodenitrogenation (HDN).[1−3] The HDN process using pyridine as an example is shown in eq 1a, with previously estimated values in black and red, and calculated values in blue.[4]

The three individual steps that comprise the net HDN reaction (eqs 1b−1d) are exothermic; $\Delta_r H^{\circ}$ values in eq 1b all agree, and this is the reaction described in this article. The HDN reaction is slow in the absence of a catalyst, and heterogeneous or nanoparticle catalysts have been studied.[1−3,5] In addition to a model for the HDN reaction, the removal of

$$NC_5H_{5(g)} + 5\,H_{2(g)} = NH_{3(g)} + C_5H_{12(g)} \qquad \Delta_r H^{\circ} = -86.5,\ -66.3,\ -80.3\ \text{kcal mol}^{-1} \quad (1a)$$

$$NC_5H_{5(g)} + 3\,H_{2(g)} = HNC_5H_{10(g)} \qquad \Delta_r H^{\circ} = -47.5,\ -47.9,\ -48.4\ \text{kcal mol}^{-1} \quad (1b)$$

$$HNC_5H_{10(g)} + H_{2(g)} = H_2NC_5H_{11(g)} \qquad \Delta_r H^{\circ} = -9.0,\ -19.0,\ -15.3\ \text{kcal mol}^{-1} \quad (1c)$$

$$H_2NC_5H_{11(g)} + H_{2(g)} = NH_{3(g)} + C_5H_{12(g)} \qquad \Delta_r H^{\circ} = -21.0,\ -34.6,\ -17.7\ \text{kcal mol}^{-1} \quad (1d)$$

pyridine holds a specific place in industrial applications. For example, pyridine inhibits heterogeneous catalysts involved in fuel reforming[6] and poisons acid catalysts[7] and therefore must be eliminated from the feedstocks. For synthetic applications, hydrogenation of pyridine affords straightforward synthetic routes to high-value piperidine derivatives, particularly in its

asymmetric version.[8] As far as we know, only heterogeneous catalysts are known to catalyze this transformation, and no homogeneous catalyst has been reported; however, functionalized pyridines and bicyclic derivatives of pyridines have been hydrogenated by various homogeneous catalysts,[9,10] but pyridine itself does not appear on the list of substrates that are used. A kinetic law has been determined in the case of molybdenum-based catalyst,[11] and the binding mode and reactivity of pyridine to a platinum surface has been studied.[12,13] A computational study of the initial hydrogenation steps of pyridine at MoP(001) indicated that several pathways are possible.[14]

The mechanism of the heterogeneous reactions is speculative, and soluble organometallic compounds have been studied as catalysts in order to develop mechanistic models from kinetic and labeling studies.[15−17] The bulk of the mechanistic studies in the literature involve d-block transition metals with either d^6 or d^8 electronic configuration and use quinoline as a model heterocycle. The enthalpy change for hydrogenation of quinoline is less exothermic than for pyridine (eqs 2a and 2b; estimated and calculated values are in black and blue, respectively).[4]

$$\Delta_r H° = -32, \text{-31.6 kcal mol}^{-1} \quad (2a)$$

$$\Delta_r H° = -41, \text{-33.2 kcal mol}^{-1} \quad (2b)$$
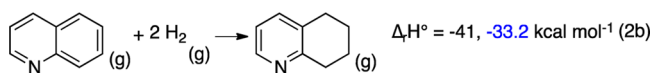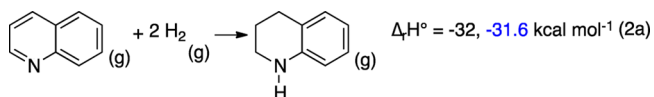
The postulated mechanisms differ mainly in the first addition of H_2 to the C=N double bond; the mechanisms are classified as (i) inner-sphere or (ii) outer-sphere processes. The inner-sphere process begins by hydride transfer across the C=N double bond followed by H_2 addition across the M−N(amide) bond resulting in the formation of an amine and a metal hydride.[18−21] The outer-sphere mechanism begins by proton transfer from an η^2-H_2 complex or from HX in an ionic hydrogenation step, generating a cationic amine that is not coordinated to the metal hydride fragment; hydride transfer results in reduction of the C=N double bond.[17,22−26]

It is not straightforward to extend the mechanistic knowledge developed from these studies to lanthanide hydride catalyzed hydrogenation reactions because, for example, Cp′$_2$CeH is not likely to undergo reductive elimination and/or oxidative addition cycles or to form η^2-H_2 adducts. Nevertheless, Cp′$_2$CeH does indeed reduce pyridine to piperidine under mild conditions, the mechanism of which is the focus of this article.

The first reported apparently homogeneous catalytic hydrogenation of pyridine to piperidine using a d transition metal was reported some 45 years ago, using RhCl$_3$(py)$_3$ with NaBH$_4$ and H_2 in dimethylformamide as the solvent.[27] Although no mechanism was proposed, the rate of the first equivalent of H_2 was slower than the second and third equivalents. A second study reported hydrogenation of 2-methylpyridine to 2-methylpiperidine catalyzed by [Cp*Rh(NCMe)$_3$]$^{2+}$ at a partial pressure of 27 atm of H_2 at 40 °C.[28] These authors showed that when D_2 was used, deuterium is incorporated into the CH$_2$ and CH$_3$ groups of the resulting product; however, the reaction mechanism remained obscure.

In the context of pyridine hydrogenation, it is noteworthy that Ru(PCy$_3$)$_2$(η^2-H$_2$)$_2$(H)$_2$ does not hydrogenate pyridine

(3 atm, 80 °C) even though it does hydrogenate benzene.[29] In addition, partial stoichiometric hydrogenation of pyridine was achieved when V[N(SiMe$_3$)$_2$][N(SiMe$_3$)Si(Me)$_2$CH$_2$](py) was exposed to H_2 (27 atm, 20 °C) because V[(N(SiMe$_3$)$_2$]$_2$(4,5,6-trihydropyridyl)(py) was isolated.[30]

This article describes a homogeneous reduction of pyridine mediated by (1,2,4-(Me$_3$C)$_3$C$_5$H$_2$)$_2$Ce(η^2-NC$_5$H$_4$) and H_2 (Scheme 1), where [Ce]′ refers to the (1,2,4-(Me$_3$C)$_3$C$_5$H$_2$)$_2$Ce fragment.

**Scheme 1. Hydrogenation of Pyridine to Piperidine**
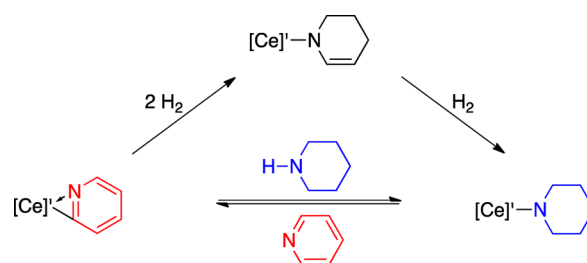
■ RESULTS

1. General Outline. The chemical reactions involved in hydrogenation of pyridine to piperidine are illustrated in Scheme 1. The trihydropyridyl and the piperidyl metallocenes are isolated when Cp′$_2$Ce(2-pyridyl) (**1**) is exposed to H_2, and they are prepared by independent synthesis. These metallocenes are characterized in the solid state (X-ray crystallography for the trihydropyridyl and piperidyl complexes) and in solution (^{1}H NMR spectroscopy). The reaction chemistry of these three metallocenes is developed with a focus on proposing a mechanism for the homogeneous hydrogenation reaction. Computational studies follow the experimental studies and provide a molecular level of understanding of the hydrogenation reaction.
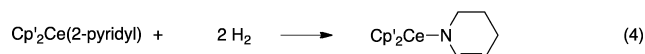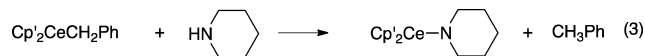
2. Hydrogenation of Pyridine to Piperidine. The conversion of pyridine to piperidine involves the addition of pyridine to a solution of Cp′$_2$CeH, followed by the addition of H_2. The products that form depend on the partial pressure of H_2 and temperature. When **1** is dissolved in pentane and placed under 12 atm of H_2 for 2 days at 20 °C, conversion to the trihydropyridyl complex is only partially complete because the ratio of pyridyl to trihydropyridyl is 2:3. Stirring for 7 days increases the amount of the piperidyl compound; the ratio of pyridyl/trihydropyridyl/piperidyl is 3:18:1. When the latter solution is cooled, trihydropyridyl crystallizes as brown-purple crystals in 27% yield. Another synthetic route to the trihydropyridyl compound involves stirring a mixture of **1** and Cp′$_2$CeH, in a mole ratio of 1:0.05, under H_2 (1 atm) in pentane for 13 days. Crystallization by cooling affords the trihydropyridyl complex in 80% yield. If Cp′$_2$CeH is omitted, the conversion is slow at 20 °C; by ^{1}H NMR spectroscopy, the ratio of pyridyl/trihydropyridyl/piperidyl is 12:1:20 after 192 days. When Cp′$_2$Ce(4-methyl-2-pyridyl) is exposed to H_2 (12 atm) at 20 °C in pentane, no hydrogenation occurs when this mixture is stirred for 7 days.

3. Synthesis of 1 and Related Amides. Three synthetic routes for **1** are shown in Scheme 2. The reactions of a metallocene hydride or alkyl with pyridine are the traditional synthesis routes for orthometallated pyridine derivatives.[31−35] A direct synthesis using pyridine as the solvent is a useful multigram synthesis for this starting material. The red 2-pyridyl

Scheme 2. Synthesis of 1 and Its Exchange Reaction with Labeled Pyridine-d_5
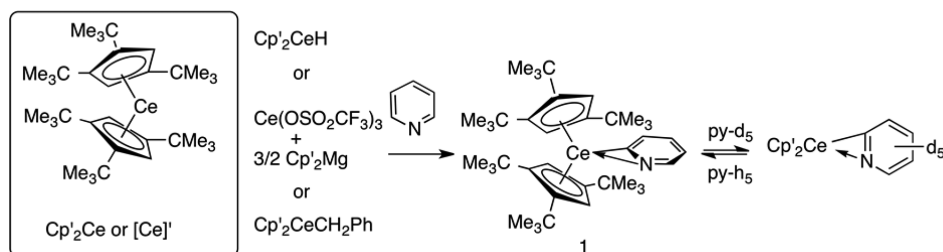
derivative is crystallized from pentane, melts at 256−260 °C, and affords a monomeric molecular ion in the mass spectrum.

The substituted 2-pyridyl derivatives are prepared by analogous reactions in order to assign the ^{1}H NMR resonances in **1** (Table 1). The pyridyl resonances in the ^{1}H NMR

Table 1. ^{1}H NMR Chemical Shifts, at 20 °C in C_6D_6[a]

Compound	H_α	H_β	H_γ	H_δ
(α,β,γ,δ-pyridyl)	14.0	14.3	11.6	5.0
	d, J = 6	t, J = 7	d, J = 6	$\nu_{1/2}$ = 200
(4-Me)	14.2	5.13 (CH3)	11.9	5.5
	$\nu_{1/2}$ = 8		$\nu_{1/2}$ =7	$\nu_{1/2}$ = 12
(6-Me)	15.0	15.4	12.3	−3.4 (CH$_3$)
	$\nu_{1/2}$ = 16	$\nu_{1/2}$ = 16	d, J = 7	
(3-Me)	3.8 (CH$_3$)	15.4	12.4	6.1
		d, J = 7	d, J = 7	$\nu_{1/2}$ = 13
(5-Me)	14.5	14.5	3.6 (Me)	5.4
				$\nu_{1/2}$ = 9

[a]Chemical shifts in δ units; $\nu_{1/2}$ and coupling constants in Hz.

spectrum contain four chemically inequivalent CH's. The triplet at δ_H = 14.3 is assigned to H_β because this resonance is absent in the corresponding 4-methylpyridine derivative and replaced by the methyl group resonance at δ_H = 5.13. The broad resonance near δ_H = 5 is assigned to H_δ because this resonance is absent in the corresponding pyridyl when 2-methylpyridine is used and replaced by a methyl resonance at δ_H = −3.4. These two assignments are clear, but those for H_α and H_γ are less clear and could be reversed because the assignment in the two isomers resulting from 3-methylpyridine cannot be made unequivocally. In addition to the η^2-pyridyl resonances, the Cp′-CH resonances are observed as a pair of resonances, δ_H ≈ 21 and 25 due to 2H each, and three Me$_3$C resonances in a 18:18:18 ratio in the neighborhood of 0, −2, and −8, respectively. The 20 °C NMR spectra show that these 2-pyridyl metallocenes have C_s symmetry. The other two amide derivatives, Cp′$_2$Ce(piperidyl) and Cp′$_2$Ce(4,5,6-trihydropyridyl), are prepared as shown in eqs 3 and 4, respectively. The two metallocenes are important because they lie on the pyridine-to-piperidine hydrogenation pathway. Both compounds are

$$Cp'_2CeCH_2Ph \; + \; HN\bigcirc \longrightarrow Cp'_2Ce-N\bigcirc \; + \; CH_3Ph \quad (3)$$

$$Cp'_2Ce(2\text{-pyridyl}) \; + \; 2\,H_2 \longrightarrow Cp'_2Ce-N\bigcirc \quad (4)$$

crystallized from pentane and are structurally characterized by X-ray crystallography (see section 5).

4. Variable-Temperature ^{1}H NMR Studies. As noted above, the 20 °C ^{1}H NMR spectrum of **1** indicates that it has C_s symmetry; however, it is fluxional, as shown by the temperature dependence of the resonances illustrated in the δ versus T^{-1} plots (Figure 1). At temperatures greater than 315 K ($1/T$ = 0.0032), the Me$_3$C resonances appear in a ratio of 36:18 and the Cp′-CH resonances are broadened into the baseline, but they are observed as a single broad resonance by 360 K, consistent with the Cp′$_2$Ce fragment having average C_{2v} symmetry at high temperature. As the temperature is lowered, the Me$_3$C resonance (36H) decoalesces and appears as a pair of broadened resonances at T ≈ 300 K, and the Cp′-CH's resonances are two very broad features (Figure 1A,B). As the temperature is lowered further, all six Me$_3$C groups become inequivalent by ≈215 K ($1/T$ = 0.00465) and Cp′-CH are also inequivalent, indicating that each of the Cp′ rings in the Cp′$_2$Ce fragment are chemically inequivalent. The chemical shifts of the 2-pyridyl ring hydrogen atoms are only slightly temperature-dependent and essentially linear in T^{-1} (Figure 1C). The high-temperature spectra show that the Cp′ rings are free to rotate about their pseudo-C_5 axes, generating average C_{2v}-symmetry spectra. As the temperature is lowered, a plane and the C_2 axis are lost, the top and bottom Cp′ rings are equivalent, and the individual Me$_3$C groups on a given ring are inequivalent. As the temperature is lowered further, all symmetry operations are removed and the top and bottom Cp′ rings become inequivalent. A structure that fits the low-temperature spectra requires that the planar η^2-pyridyl ligand does not lie in the plane that is the bisector of the C_t−Ce−C_t angle (C_t = Cp′ ring centroid), resulting in a molecule with C_1 symmetry. A similar temperature behavior was observed in Cp′$_2$Ce(η^2-CH$_2$OCH$_3$), and a similar explanation was suggested; that is, the orientation of the η^2-CH$_2$OCH$_3$ moiety is oblique to the C_t−Ce−C_t plane.[36]

The temperature dependence of the ^{1}H NMR chemical shifts of the piperidyl ligand resonances in Cp′$_2$Ce(piperidyl) are complicated by axial−equatorial site exchange in the six-membered ring. At 373 K, in C_7D_{14}, the piperidyl resonances are observed as two single resonances at δ_H = 12.23 and 6.78 in a ratio of 4:6 and the Cp′ resonances are observed at δ_H = 19.72, 2.0, and −9.85 in a ratio of 4:36:18, respectively. At this temperature, Cp′$_2$Ce(piperidyl) has average C_{2v} symmetry and axial−equatorial site exchange is rapid; the ratio of 4:6 implies that the β- and γ-CH$_2$ resonances are accidentally degenerate. As the temperature is lowered to 308 K, the
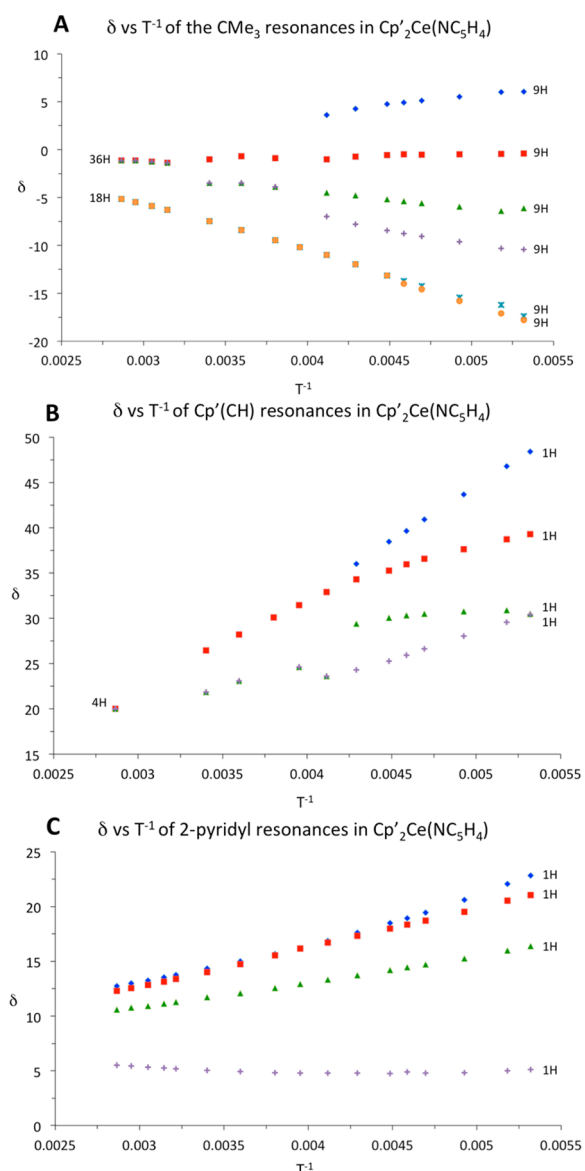
Figure 1. Variable-temperature ^{1}H NMR chemical shifts for **1**, with δ in parts per million and T in Kelvin. The label nH (n = 1 or 9) refers to the relative number of hydrogens.

piperidyl resonances are observed as four resonances at $\delta_H \approx$ 15.3, 9.5, 8.3, and 7.3 due to 2H each, a resonance due to 2H is hidden, and the Cp′ resonances appear at $\delta_H \approx$ 24.7, 21.9, 4.6, −2.4, and −14.2 in a area ratio of 2:2:18:18:18, implying that axial−equatorial site exchange is slow and the molecule has either C_2 or C_s symmetry. Cooling further results in a broadening of the piperidyl ligand into the baseline, from which they emerge by 225 K at $\delta_H \approx$ 44.9, 34.9, 17.8, 14.8, 14.4, 11.3, and 10.9 in a ratio of 1:1:1:1:1:2:2; one resonance due to 1H remains hidden. This pattern is maintained upon cooling to 195 K, although the chemical shifts change with the temperature. This pattern implies that the piperidyl ligand has C_1 symmetry and the axial and equatorial CH's are pairwise inequivalent, except when the chemical shift difference between them is too small to resolve given the line width of the individual resonances. However, the Cp′ resonances maintain their 2:2:18:18:18 pattern to 195 K; the δ_H versus T^{-1} plots are available in the Supporting Information (SI).

The assignment of the piperidyl ligand resonances is confirmed by preparing Cp′$_2$Ce(piperidyl-d_{10}) and observing

the temperature dependence of the ^{2}H NMR spectra; the δ versus T^{-1} plots are available in the SI. At 368 K, the spectrum consists of two resonances at δ_D = 12.8 and 7.0 in a ratio of 4:6. As the temperature is lowered, these resonances shift and broaden; by 308 K, four resonances are observed at $\delta_D \approx$ 15.5, 9.4, 8.4, and 7.5 in a ratio of 2:2:2:2. By 215 K, six very broad resonances are observed at 46, 36, 18, 17, 15, and 12 in the approximate ratio of 1:1:1:1:1:4. Although the ^{2}H NMR pattern mirrors the ^{1}H NMR and supports the assignment, the line widths and therefore the resolution of the individual resonances is not observed at low temperature.

In 4-methylpiperidine, the methyl group in the γ site changes the relative free energy of the conformers in which the methyl group is either axial or equatorial. The conformer in which the methyl group is equatorial is more stable than the axial conformer[37] by 1.9 kcal mol^{-1}, and each conformer has C_s symmetry. This energy difference between the conformers in 4-methylpiperidine simplifies the ^{1}H NMR spectra of Cp′$_2$Ce(4-methylpiperidyl). At 308 K, the 4-methylpiperidyl ligand resonances are observed at $\delta_H \approx$ 27.7, 21.5, 11.6, 11.4, 8.9, 8.4, 7.1, and 4.12, all due to 1H, except the resonance at 7.1 due to 2H and the resonance at 4.12 due to 3H, assigned to the 4-Me group; again a resonance due to 1H is hidden. This pattern is maintained to T = 213 K (Figure 2). The pairwise inequivalence of the α-H and β-H resonances in the six-membered ring shows that the ligand has C_1 symmetry and the piperidyl ligand is top-bottom and left-right inequivalent. A possible explanation for this asymmetry is that the piperidyl ligand has an oblique orientation over the temperature range, as found in the solid-state crystal structure of the piperidyl derivative (see section 5), illustrated by the Newman projection down the N−Ce bond where the Me$_3$C groups closer to the piperidyl ring are illustrated in red (Scheme 3). The δ versus T^{-1} plot (Figure S1 in the SI) shows that the Cp′$_2$Ce fragment has C_2 or C_s symmetry, implying that the 1,2,4-(Me$_3$C)$_3$C$_5$H$_2$ ligands are able to librate about their pseudo-C_5 axes but the piperidyl ligands do not have this freedom.

The pattern outlined above is maintained when the piperidyl ligand is replaced by the 4,5,6-trihydropyridyl ligand in which the α-carbon atoms are inherently left-right asymmetric. The variable-temperature ^{1}H NMR spectra of isolated Cp′$_2$Ce-(4,5,6-trihydropyridyl) show that the ring Me$_3$C groups appear in a 36:18 ratio and the ring CH's are chemically equivalent at high temperature but in 18:18:18 and 2:2 ratios, respectively, at 194 K; a δ versus T^{-1} plot is available in the SI (Figure S2). At 368 K, the ligand resonances are in a 1:2:2:2:1 ratio, indicating that axial−equatorial site exchange of the CH$_2$ groups is rapid at this temperature. As the temperature is lowered, the resonances broaden, disappear into the baseline, and reappear by 260 K ($1/T$ = 0.00385) as six resonances of 1H each. The downfield CH resonance, presumably the α-olefinic one, monotonically moves downfield as the temperature is lowered, while the other, presumably the olefinic β-CH resonance, monotonically moves upfield, and both resonances follow Curie law. This pattern indicates that axial−equatorial site exchange is slow at this temperature, and as observed in the piperidyl case, the resonance assigned to the α-olefinic CH moves steadily downfield as the temperature is lowered.

5. Solid-State X-ray Crystallographic Studies. An ORTEP of the fully hydrogenated derivative [1,2,4-(Me$_3$C)$_3$-C$_5$H$_2$]$_2$Ce(NC$_5$H$_{10}$) is shown in Figure 3. Crystal data are in the Experimental Section and Supporting Information, and some important bond distances and angles are given in Table 2.
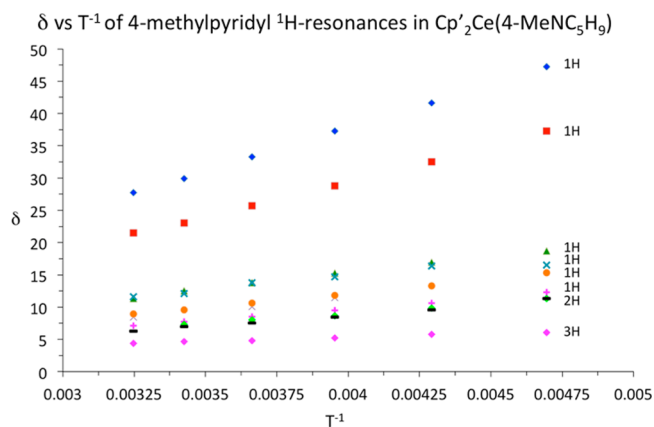
δ vs T⁻¹ of 4-methylpyridyl ¹H-resonances in Cp′₂Ce(4-MeNC₅H₉)

Figure 2. Variable-temperature δ versus T^{-1} plot for the 4-methylpiperidyl ligand resonances in Cp′₂Ce(4-MeNC₅H₉), with δ_H in parts per million and T in Kelvin. The label nH (n = 1, 2 or 3) refers to the relative number of hydrogens.

Scheme 3. Newman Projection of Cp′₂Ce(piperidyl), Showing Only the Orientation of the α-CH₂ Groups of the Piperidyl Ligand, down the N−Ce Bond
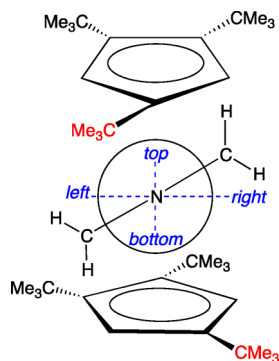
The bond distances and angles for the Cp′₂Ce fragment in both structures are in the range found in related Cp′₂CeX compounds in which the average Ce−C(Cp′) distances vary from 2.81 ± 0.05 to 2.86 ± 0.05 Å; the range of the individual Ce−C(Cp′) distances is large, resulting in the large value of the average deviation from the mean in these bent sandwich

Table 2. Selected Bond Distances (Å) and Angles (deg) in Cp′₂Ce(NC₅H₁₀) (13) and Cp′₂Ce(NC₅H₈) (9)[a]

	Cp′₂Ce(NC₅H₁₀)	Cp′₂Ce(NC₅H₈)
Ce−C(Cp′) ave	2.86 ± 0.06	2.84 ± 0.05
Ce−C(Cp′) range	2.769(1)−2.930(1)	2.754(3)−2.910(3)
Ce−C_t	2.60	2.56
Ce−N	2.269(1)	2.327(3)
N−C35	1.453(2)	1.352(5)
N−C39	1.450(2)	1.451(5)
Ce⋯C35	2.997(1)	2.966(4)
Ce⋯H59	2.67(1)	
Ce⋯H35		2.79(1)
C_t−Ce−C_t	140	143
C_t−Ce−N	110, 110	110, 110
Ce−N−C35	105.1(1)	104.3(2)
Ce−N−C39	145.1(1)	138.6(3)
C35−N−C39	109.6(1)	112.9(3)

[a]Atom numbers refer to the ORTEPs in Figures 3 and 5.

metallocenes. The average Ce−C(Cp′) distance of 2.86 ± 0.06 Å lies at the longer end of the range and is associated with a metallocene in which the X ligand is not monodentate but an η^2-X−L ligand. The Ce−N distance in **13** is 2.269(1) Å and somewhat shorter than the Ce−N distances in Cp*Ce[N(SiMe₃)₂]₂ of 2.352 ± 0.003 Å,[38] 2.317 ± 0.012 Å in Ce(NC₅H₁₀)₃(thf),[39] and 2.33(4) Å in the gas-phase electron diffraction structure of Ce[N(Si(Me₃)₂]₃.[40] The (Me₃C)₃C₅H₂ rings in the piperidyl metallocene are related by a C_2 axis collinear with the Ce−N bond, although the Ce−N vector lies off the C_2 axis by ca. 4°. The geometry at nitrogen is planar, but Ce−N−C35 and Ce−N−C39 are not 120° but 105.1(1)° and 145.1(1)°, respectively. The angular asymmetry results in a short Ce⋯C35 contact distance of 2.997(1) Å, 0.026 Å shorter than the Ce⋯C(ipso) contact distance in Cp′₂Ce(η^2-CH₂Ph),[41] resulting in a Ce⋯H59 contact distance of 2.67(1) Å; the Ce⋯H60 distance is 3.60(1) Å, and the Ce⋯C35−H59 angle is 61°. These values may be compared with those at the more open Ce−N−C39 angle in which the Ce⋯C39 distance is 3.56 Å. The piperidyl ligand adopts a chair conformation in which the C35−N−C39 angle of 109.6(1)° is identical with that found in the gas-phase electron diffraction structure of piperidine of 111(2)° and the

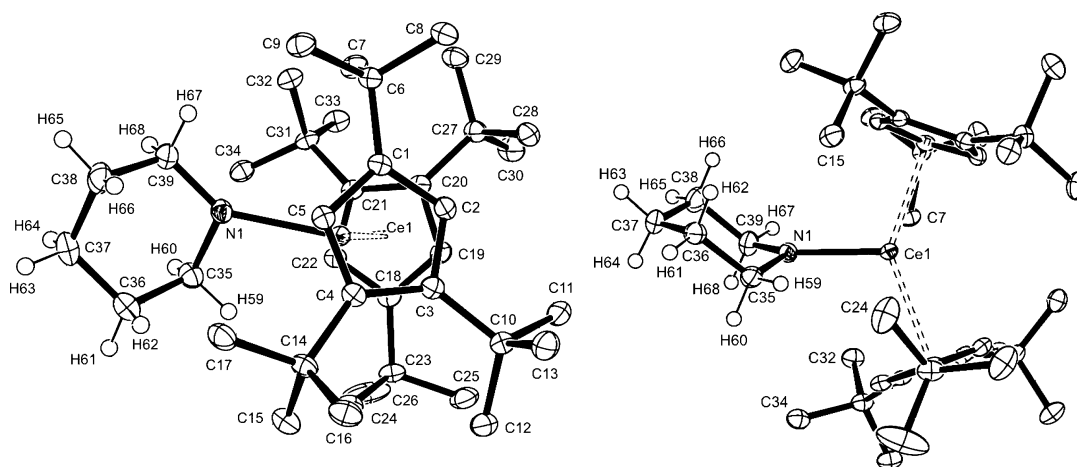**Figure 3.** ORTEPs (top and side views) of [1,2,4-(Me₃C)₃C₅H₂]₂Ce(NC₅H₁₀). 50% thermal ellipsoids for the non-hydrogen atoms that are refined anisotropically, and all hydrogen atoms are located and refined isotropically and represented by spheres of arbitrary volumes. This complex will be labelled **13** in the Computational Section.

N−C35 and N−C39 distances of 1.453(2) and 1.450(2) Å, respectively, are close to the equivalent distances in piperidine of 1.471(3) Å.[42] As mentioned above, the Ce−N vector lies off the C_2 axis by 4°, the Ce−N−C angles are asymmetric, and the plane defined by C35−N−C39 does not lie on the bisector plane of the C_t−Ce−C_t wedge but is rotated out of this plane by 19°. Thus, the piperidyl ligand lies in a pocket defined by C9, C17, C24, and C34, the four carbon atoms of four methyl groups oriented toward the open face of the metallocene wedge. This molecular asymmetry is deduced from the solution ^{1}H NMR spectra but better defined by the solid-state crystal structure.

A more difficult question, however, is why the molecule distorts in such a way that it develops short Ce···C35 and Ce···H59 contact distances. An initial proposition is that the Ce···C35−H59 contact is due to an "agostic" Ce···H−C bond.[43−49] If true, then the C35−H59−H60 bond distances and angles within the piperidyl ligand should be significantly different from those at C39−H67−H68. These internal comparisons are tabulated in Table S1 in the SI; given the uncertainty in the hydrogen-atom positions, there is no significant difference between the bond distances and angles at C35 and C39, which argues strongly against the proposition of an agostic Ce···H−C interaction. If the C−H distances and H−C−H angles are not perturbed by the Ce···C(H) contact distance, then geometric constraints resulting from the manner in which the piperidyl fits into the pocket defined by the orientation of the Me$_3$C groups on the Cp′ rings are an alternative proposition (see Scheme 3). Examination of the H···H contact distances between the piperidyl ligand and the ring Me$_3$C groups range from 2.26 to 3.48 Å, some of which are close to the sum of the van der Waals radius of two hydrogen atoms of 2.4 Å[50] (Figure 4, left). Some of these short contacts would undoubtedly be shorter if the orientation of the piperidyl ligand were symmetric, with C_α−N−C_α angles of 120°, and the plane, defined by Ce−N−C_α, was oriented perpendicular to the C_t−Ce−C_t plane. The deduction that the asymmetric distortion results from intramolecular steric repulsions between the Cp′ Me$_3$C groups at the front of the metallocene wedge and the CH's of piperidyl ligand seems inescapable.

The ORTEP of [1,2,4-(Me$_3$C)$_3$C$_5$H$_2$]$_2$Ce(NC$_5$H$_8$) is shown in Figure 5, selected bond distances and angles are given in Table 2, and crystal data are in the SI. The crystal data show that **13** and **9** crystallize in the same crystal system in space group $C2/c$. The average Ce−C(Cp′) bond length for the trihydropyridyl complex is slightly shorter than that in **13**; the individual Ce−C distances are shorter by 0.020 Å. In contrast, the Ce−N distance of 2.327(3) Å in the trihydropyridyl complex is significantly longer than that found in the fully hydrogenated case of 2.269(1) Å. As in **13**, the Ce−N−C35 angle is less than the Ce−N−C39 angle, 104.3(2)° and 138.6(3)°, respectively, and the Ce−N vector is off the C_2 axis by 10°, moving C35−H35 close to cerium; the Ce···C35 and Ce···H35 contact distances are 2.966(4) and 2.79(1) Å, respectively. The orientation of the Me$_3$C groups on the individual rings is identical in both structures, and the tilt of the plane defined by C35−N−C39 relative to the perpendicular bisector of C_t−Ce−C_t is 28°. As in the piperidyl structure, the NC$_5$H$_8$ ligand sits in the pocket defined by the Me$_3$C methyl groups C7, C12, C24, and C26 on the open side of the metallocene wedge in the orientation illustrated in Figure 4, right, which shows the pattern of short H···H contact distances that range from 2.22 to 2.98 Å between the hydrogen atom of
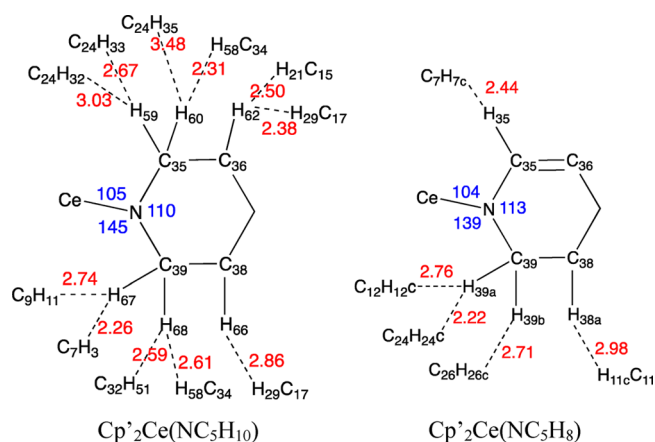

Figure 4. Distances in Å, shown in red, between hydrogen atoms on the amide ligands and the ring Me$_3$C groups. Angles in degrees around the nitrogen atoms are shown in blue. The atom numbering is the same as used in Figure 3 for **13** and Figure 5 for **9**.

the trihydropyridyl ligand and the hydrogen atoms on the ring Me$_3$C groups.

The geometries at C35 and C39 in the piperidyl ligand (Figure 3 and Table S1 in the SI) are identical with those at C39 in the trihydropyridyl ligand (Figure 5), supporting the proposition argued above, viz., that the asymmetry in the Ce−N−C angles and the resulting short Ce···C distances in both structures are dictated by the H···H interactions between the Cp′ rings and the amide ligands, illustrated in Figure 4. The asymmetry in both structures persists in solution, showing that the asymmetry is a molecular property.

The trihydropyridyl ligand has a half-chair conformation, as observed in cyclohexene, because the four carbon atoms of the amido ligand are essentially coplanar, as indicated by the C35−C36−C37−C38 torsion angle of −6.4°. Relative to the piperidyl complex, the Ce−N bond is elongated by 0.058 Å, a possible explanation of which is that conjugation of the nitrogen lone pair with the vicinal π* orbital reduces the electron density on nitrogen, which lengthens the Ce−N bond distance.

6. Mechanistic Studies. The synthetic studies outlined in section 2 show that the presence of a small amount of Cp′$_2$CeH increases the rate of the hydrogenation reaction. In order to document the catalytic effect, a solution of **1** is prepared in C$_6$D$_{12}$ and equal volumes of the solution are placed into two NMR tubes. To one NMR tube is added Cp′$_2$CeH, the mole ratio of **1** to Cp′$_2$CeH is 10:1, H$_2$ (1 atm) is added to both NMR tubes, and the progress of the reaction is monitored by ^{1}H NMR spectroscopy. The sample without added Cp′$_2$CeH after 20 min at 20 °C is unchanged. After heating to 60 °C for 2 days, the ratio of **1**/trihydropyridyl is 16:1. After 4 days, some piperidyl complex forms and the ratio of **1**/trihydropyridyl/piperidyl is 145:15:1, and after 10 days at 60 °C, the ratio is 30:6:1. After 180 days at 60 °C, the resonances due to **1** are absent and the ratio of trihydropyridyl/piperidyl is 1:6. In contrast, the NMR tube with added Cp′$_2$CeH begins to form some trihydropyridyl after 20 min at 20 °C, and the ratio of **1**/trihydropyridyl is 5:1. After heating to 60 °C for 2 days, all of **1** is converted to trihydropyridyl. After 4 days, the piperidyl complex begins to form and the ratio of trihydropyridyl/piperidyl is 30:1, and after 10 days, the ratio is 6:1. These semiquantitative experiments show that Cp′$_2$CeH promotes the addition of the first, and/or second, or both H$_2$ addition steps.
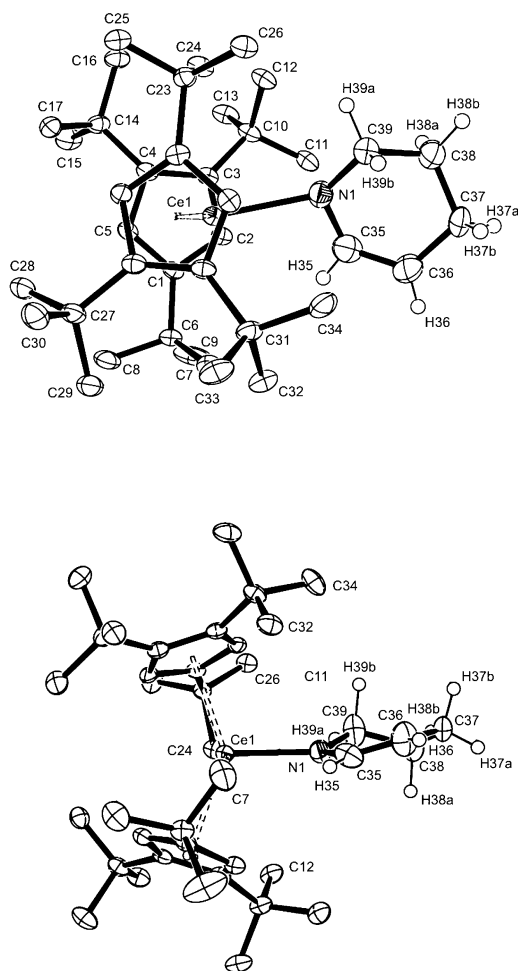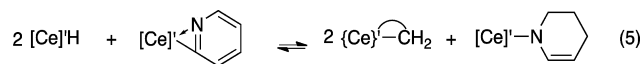
Figure 5. ORTEPs (top and side views) of [1,2,4-(Me₃C)₃C₅H₂]₂Ce-(NC₅H₈). 50% thermal ellipsoids on the non-hydrogen atoms that are refined anisotropically. The hydrogen atoms on the NC₅H₈ ring are located and refined isotropically and shown as spheres of arbitrary volumes, but those on the Cp′ ring are placed in calculated positions and not refined. This complex will be labelled **9** in the Computational Section.

In order to answer the question about the role of Cp′₂CeH on the rate of the third hydrogenation step, a similar set of two NMR tubes are prepared with equal concentrations of the trihydropyridyl complex in C₆D₁₂. Some Cp′₂CeH is added to one NMR tube, the ratio of the trihydropyridine to Cp′₂CeH is 8:1, H₂ is added to both NMR tubes (1 atm), and the resonances are monitored by ¹H NMR spectroscopy. The sample without added Cp′₂CeH is heated to 60 °C; after 1 day, the ratio of trihydropyridyl/piperidyl is 4:1, after five days, 1:1, and after 19 days, 1:2. The change is similar for the sample with added Cp′₂CeH because the ratio of trihydropyridyl/piperidyl is 6:1, after five days, 5:4, and after 19 days, 1:3. This set of experiments shows that the last addition of H₂ is not greatly influenced by the presence of deliberately added Cp′₂CeH, in contrast to the first two additions.

Dissolving **1** in pyridine-d_5 and monitoring the progress of the reactions is followed by ¹H NMR spectroscopy, using the change in the upfield Me₃C resonance relative to the four 2-pyridyl resonances. At the beginning, the ratio is 18:4, after 2 days at 20 °C, it is 27:4, after 5 days, it is 180:4, and after 9 days, all of the 2-pyridyl-h_4 resonances are absent from the ¹H NMR spectrum and replaced by the 2-pyridyl-d_4 resonances (²H NMR). When this mixture is heated to 60 °C for 1 day,

the ratio of ¹H NMR resonances due to Me₃C relative to those in the ortho, meta, and para sites of pyridine are 7:2:2:1, respectively. After 6 days at 60 °C, the ratio is 4:4:2:1, and after 14 days, the ratio is 2:6:2:1. This experiment indicates that exchange of coordinated 2-pyridyl with labeled pyridine occurs and the deuterium that enters the Me₃C site exchanges exclusively with the ortho site in pyridine at 20 °C. Heating the solution results in deuterium for hydrogen exchange from the Me₃C-d_x group into the ortho sites of pyridine, exclusively. Exchange of hydrogen for deuterium at the ortho site in 2-pyridyl is also shown by exposing **1** to an atmosphere of D₂; deuterium is found only in the ortho site. These exchange experiments show that the 2-pyridyl exchanges with pyridine and the ortho sites in 2-pyridyl exchange with the Me₃C groups on the Cp′ ring, presumably by metallacycle formation.

Although the metallacycle, {**Ce**}′-**CH₂**, reacts rapidly with H₂ and therefore cannot play a significant role in the hydrogenation reaction, in the *absence* of added H₂, it does play a role, as documented in the following experiments. In a NMR tube, **1** and Cp′₂CeH are dissolved in C₆D₁₂ at 20 °C. After 20 min, only these two metallocenes are present in a 1:2 ratio (eq 5). After 3 days at 20 °C, the trihydropyridyl and metallacycle resonances appear; the ratio of **1**/Cp′₂CeH/trihydropiridyl/metallacycle is 9:27:2:1. After 2 days at 60 °C, the ratio is 2:5:1:1, and after 7 days, 1:3:1:1, and this ratio does not change for 16 days. After this time, the NMR tube is evacuated, the atmosphere is

$$2 \; [\text{Ce}]'\text{H} \;\; + \;\; [\text{Ce}]' \overset{N}{\underset{}{\diagdown}} \quad \rightleftharpoons \quad 2 \; \{\text{Ce}\}' \overset{\frown}{-} \dot{\text{C}}\text{H}_2 \;\; + \;\; [\text{Ce}]' \text{---N} \overset{\frown}{\underset{\smile}{\bigcirc}} \quad\quad (5)$$

replaced by H₂ for 5 min then reevacuated, and the atmosphere is replaced by N₂. The ratio now is 1:3:2:0. Heating this solution to 60 °C for 1 day regenerates the hydride and metallacycle resonances. These experiments show that 2-pyridyl, [**Ce**]′-**H**, and {**Ce**}′-**CH₂** are in equilibrium, the presence of H₂ ensures that [**Ce**]′-**H** is present as 2-pyridyl is converted to trihydropyridyl, and the formation of piperidyl is slow.

Another reaction of the metallacycle is illustrated in the following experiments. A ¹H NMR tube containing trihydropyridyl and {**Ce**}′-**CH₂** in C₆D₁₂ in a 5:1 ratio is heated at 60 °C for 1 day. During this time, some **1** forms along with resonances due to Cp′₂CeH; the ratio of trihydropyridyl/{**Ce**}′-**CH₂**/[**Ce**]′-**H**/**1** is 25:5:2:1. After heating for 6 days, the ratio is 6:1:2:1. This experiment shows that dehydrogenation of the trihydropyridyl complex to **1** can occur in the *absence* of H₂. As a control, a mixture of the metallacycle, {**Ce**}′-**CH₂**, and the piperidyl complex in a 1:1.5 ratio remains unchanged after heating for 11 days at 60 °C in C₆D₁₂. When piperidyl is heated in C₆D₁₂ in an atmosphere of D₂, at 60 °C for 2 days, the Me₃C resonances in the ²H NMR spectrum are observed in a ratio 18:18:2.3, and the resonances assigned to the downfield piperidyl ligand (presumably due to the α-CH₂ groups) appear in the ²H NMR. These results are illustrated in Scheme 4.

In summary, the mechanism of homogeneous hydrogenation of pyridine to piperidyl in the presence of Cp′₂CeH and H₂ is complex because most of the elementary reactions are reversible. However, what is clear is that hydrogenation in the absence of deliberately added Cp′₂CeH is slow, and the addition of Cp′₂CeH dramatically increases the rate at least for the first two hydrogenations. Accordingly, two Cp′₂Ce units are involved: one remains attached to the pyridyl ligand and the other, in the form of Cp′₂CeH, adds to a C=C double bond. The hydride, Cp′₂CeH, is a catalyst because hydrogenolysis of

Scheme 4. Reactions of the Metallacycle with Trihydropyridyl and Piperidyl
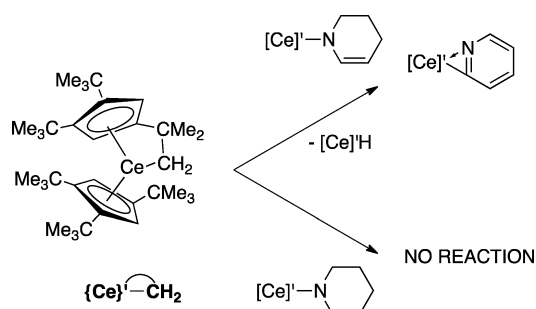
the Ce−C bond regenerates it. This specific catalytic effect and the mechanism of hydrogenation in general are explored by density functional theory (DFT) studies described next.

7. Computational Studies. *a. Computational Models.* The level of calculation needed for the possible reaction pathways is determined by a number of factors: (a) A large number of calculations are needed because of the large number of individual steps involved. It is therefore tempting to use the simplified system in which Cp′ is replaced by C_5H_5. Several test calculations showed that this strategy is inappropriate. (b) Using 1,2,4-$(Me_3C)_3C_5H_2$, Cp′, in full in the calculations introduces the problem of the large conformational space required to explore and the resulting difficulty to ensure that the best conformation of the two rings and all Me_3C groups are obtained for each extremum. Several conformers, likely to be separated by energy barriers that involve a concerted geared motion of all Me_3C groups, must be considered. To explore the conformational space in the most complete manner, several conformations based on the solid-state structures of various complexes were used as initial guesses.[36,41,51−55]

b. Pyridine Hydrogenation Pathways. Calculations reveal several possible catalytic cycles, shown in Figures 6−8, which have in common the α-metallated pyridine, **1**, and the piperidyl complex, **13**. In these Figures, the Gibbs energy values for all
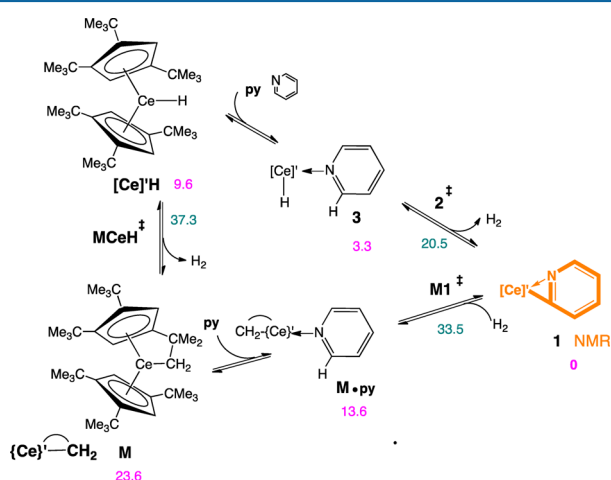
minima are indicated as pink numbers. The Gibbs energies of the transition states are color-coded in teal next to the arrows. All values are given with respect to the energy reference of **1** supplemented by the energy of all compounds necessary to maintain mass balance.

The enthalpy of hydrogenation of pyridine to piperidine, HNC_5H_{10}, is −46.3 kcal mol^{-1} without dispersion and solvation corrections and −51.4 kcal mol^{-1} when the dispersion correction is included. These values are close to the experimental enthalpy change in the gas phase of −47.5 kcal mol^{-1},[4] and the associated calculated value of ΔG is ≈ −20 kcal mol^{-1}.

A convenient way to enter the catalytic cycle is formation of the α-metallated pyridine, **1**, obtained by adding pyridine to either the hydride complex with associated loss of H_2 or to the metallacycle, **{Ce}′-CH₂**, abbreviated **M**. Both reactions are exoergic, with the pathway from the hydride by 9.6 kcal mol^{-1} and that from the metallacycle by 23.6 kcal mol^{-1} (Figure 6). These two reactions occur by way of the coordination of pyridine to the Ce fragments followed by β-CH abstraction by either the hydride or the methylene group. These two reactions have transition states that are 10.9 and 9.9 kcal mol^{-1}, respectively, above the reactants (Figure 7). The 2-pyridyl complex **1** is 3.3 kcal mol^{-1} more stable than the pyridine adduct of $Cp′_2CeH$, **3**, which is in agreement with the experimental observation that **1** forms without observation of an intermediate. However, **1** and **3** are close enough in energy and separated by a transition state of only 20.5 kcal mol^{-1} to be in equilibrium, as shown by the exchange of hydrogen for deuterium in the ortho site of pyridine.

The computed pathways for hydrogenation of pyridine are shown in Figure 7. Starting from **3**, a transition state for migrating the hydride to the carbon α to nitrogen is located with a Gibbs energy of 13.3 kcal mol^{-1}. It yields **5**, which is marginally more stable than **3**. The migration of the hydride to the other carbon atoms is calculated to be much higher in energy. To continue hydrogenation, one pathway is to form a new cerium hydride by the heterolytic addition of H_2 to **5**. The transition state **6**, which forms the hydride while adding a proton to the carbon atom adjacent to the sp^3 carbon, is found at 24.8 kcal mol^{-1}. The transition state leads to the hydride complex **7**, which is only 11.2 kcal mol^{-1} above the energy reference. To form the trihydropyridyl complex, **9**, an intramolecular transfer of the hydride is sufficient, but this step requires a transition state of 30.7 kcal mol^{-1}. The high energy of this transition state is due to the loss of the nitrogen-to-cerium dative bond required to bring the hydride close to the γ-carbon to nitrogen (see the SI for further details). This pathway clearly cannot account for the rapid formation of **9**, and an alternative pathway is explored.

An alternative pathway is to allow $Cp′_2CeH$ to add to one of the olefinic double bonds in **5**. This is a bimetallic or intermolecular pathway, where one $Cp′_2Ce$ unit remains bonded to the nitrogen while $Cp′_2CeH$ adds across a C=C double bond, forming a metallated derivative **Ce₂-7**. The addition is followed by hydrogenolysis of the Ce−C bond, regenerating $Cp′_2CeH$, accounting for its catalytic role. These two consecutive reactions form the trihydropyridyl complex **9** by way of low-energy transition states and an energetically favorable intermediate **Ce₂-7**. Repeating hydrogenation, hydrogenolysis steps on **9** yield the piperidyl complex **13** by way of a low-lying intermediate **Ce₂-11** through two low-lying transition states **Ce₂-10** and **Ce₂-12** (Figure 7).

It is possible to initiate reduction of **1** with **[Ce]′-H** followed by hydrogenolysis (**[Ce]′-H/H₂**), affording **18**. Repeating these
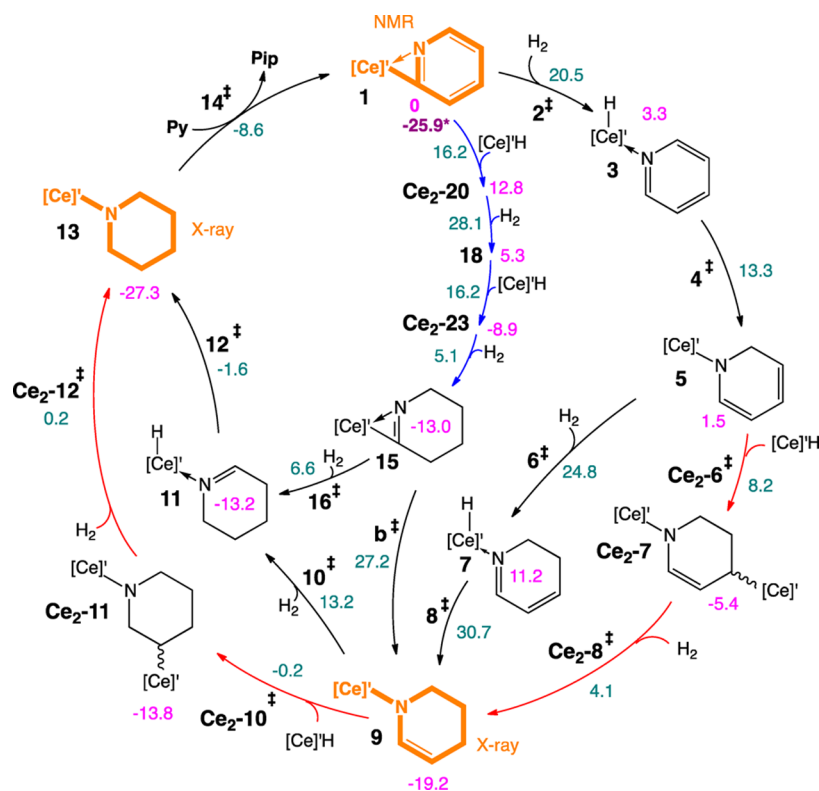

Figure 6. Gibbs energy values (kcal mol^{-1} relative to **1**) for the reaction of **[Ce]′-H** and the metallacycle **M** with pyridine **py** to form **1** and the reaction of H_2 with **M** to form **[Ce]′-H**. The transition states are labeled with the dagger sign. The H_2 and pyridine reagents that are added or eliminated in the reversible steps are indicated in either the forward or reverse directions, but not in both, in order to avoid excessive clutter in the Figure. Energies of minima and transition states are in pink and teal, respectively.

Figure 7. Reaction pathways for catalytic hydrogenation of pyridine **py** to piperidine **pip** with [Ce]′-**H**. All extrema are labeled in bold black, transition states are labeled with a dagger sign, and all energies are in kcal mol⁻¹ relative to **1**. Values for minima and transition states are in pink and teal, respectively. Adducts preceding transition states are not shown (see the SI for detailed energy profiles). The free energy of the reaction is given in bold dark pink.
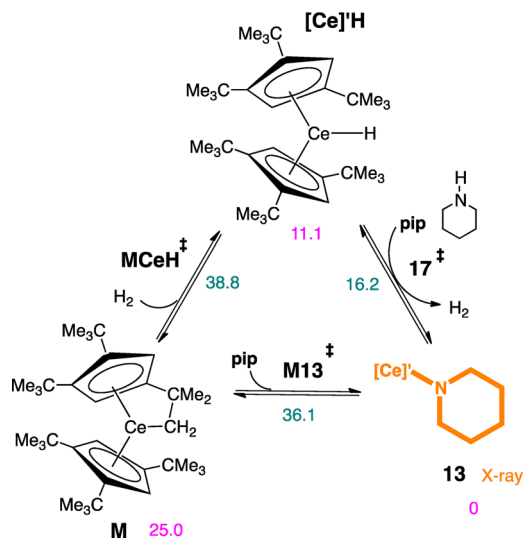

Figure 8. Free-energy profiles (kcal mol⁻¹ relative to **13**) for the reaction of piperidine **pip** with [Ce]′-**H** or the metallacycle **M** to form the piperidyl complex **13**. See Figures 6 and 7 for notations.

two reactions yields the tetrahydro derivative **15**. These two hydrogenation/hydrogenolysis pathways proceed by way of intermediates **Ce₂-20**, **18**, and **Ce₂-23**, with Gibbs energies of 12.8, 5.3, and −8.9 kcal mol⁻¹, respectively. The Gibbs energies of the transition states for the reaction of **1** with [Ce]′-**H** is 16.2 kcal mol⁻¹, which is lower than that for the addition of H₂ to **1** through transition state **2** of 20.5 kcal mol⁻¹. However, the Gibbs energy of the transition state for hydrogenolysis of the Ce–C bond in **Ce₂-20** is 28.1 kcal mol⁻¹. Hydrogenolysis

of the Ce–C bond in **15** yields **11** through a low-energy transition state **16** of only 6.6 kcal mol⁻¹, followed by intramolecular hydride transfer, which affords **13** by a low energy barrier through **12**. This pathway, **1**−**18**−**15**−**9**−**11**−**13**, has two problematic steps: (i) the high transition state for hydrogenation of **Ce₂-20** to **18** of 28.1 kcal mol⁻¹ and (ii) the step from **15** to **9** (the isolated trihydropyridyl complex) has a transition state energy of 27.2 kcal mol⁻¹ (Figure 7).

The experimental study shows that transformation of the trihydropyridyl **9** to the piperidyl **13** in the presence of H₂ is not accelerated by the deliberate addition of [Ce]′-**H**; therefore, the pathway of **9** going to **13** by way of **11** is explored. The heterolytic activation of H₂ by **9** yields **11** by way of a transition state **10** of 13.2 kcal mol⁻¹ (Figure 7). While this transition state is not particularly high in energy, in comparison to some of the highest transition states that have been located, but it is significantly higher than the transition states involving the reaction sequence [Ce]′-**H**/H₂, which are approximately 15 kcal mol⁻¹ lower. Even without the deliberate addition of Cp′₂CeH, it is likely that variable amounts of it are always present because of hydrogenolysis of the Ce–C bonds that are formed in the course of the reaction, which is likely to account for the influence of the partial pressure of H₂ on the rate of reaction.

The formation of free piperidine from the piperidyl complex **13** is initiated by coordination of pyridine to the metal center, followed by proton transfer from the Cₐ–H bond of coordinated pyridine to the nitrogen of the piperidyl complex. This proton transfer has a transition state energy at −8.6 kcal mol⁻¹, i.e., 18.7 kcal mol⁻¹ above **13**. The high energy barrier is likely due to the measured deprotonation enthalpy of the Cₐ–H bond of 399 kcal mol⁻¹, and the associated calculated bond

dissociation energy of 106 kcal mol^{-1} in pyridine.[56,57] The transformation of **13** and pyridine to **1** and piperidine is calculated to be slightly endoergic by 1.4 kcal mol^{-1} (Figure 7) and is therefore consistent with the equilibrium reaction observed experimentally through transition state **14**.

The piperidyl complex **13** is formed by the reaction of piperidine with either [**Ce**]′-**H** or the metallacycle **M**. The two reactions are exoergic, the energy barriers are modest, 5.1 kcal mol^{-1} for [**Ce**]′-**H** and 11.1 kcal mol^{-1} for **M**, and these ligand-exchange reactions complete the catalytic cycle (Figure 8).

c. Reaction of Cp′$_2$CeH with Cyclohexene. Hydrogenation and the subsequent hydrogenolysis steps are key transformations in the pathways labeled as **Ce$_2$-x**, where *x* is 6, 7, 10, 11, 12, 20, and 23 in Figure 7. Experimentally, these two steps are postulated to occur in hydrogenation of cyclohexene by Cp′$_2$CeH, a rapid reaction[58] that is a model for a tandem hydrogenation/hydrogenolysis sequence in the conversion of **5** to **9** and **13**. The transition state for insertion of the C=C double bond of cyclohexene into the Ce–H bond of Cp′$_2$CeH is located 13.3 kcal mol^{-1} above the separated reactants, Cp′$_2$CeH + cyclohexene. The following Ce–C hydrogenolysis proceeds with a barrier of only 3.8 kcal mol^{-1} with respect to the same reactants. This reaction is therefore a good model for hydrogenation of the C=C double bonds in **5**.

d. Geometrical Features of Selected Extrema. In this section, the calculated and experimental geometries are compared, keeping in mind that the calculations are, in general, for an isolated molecule in the gas phase, while the structural information is obtained for the molecules in the solid state and in solution. In general, there is good-to-excellent agreement between the experimental and computed structures. However, discrepancies arise that originate from either an inappropriate level of calculation or the use of models that are simplified representations of the experimental system.

The structure and stereochemistry of the two Cp′ rings in **1** are obtained from computations and analysis of the solution ^{1}H NMR spectra. The calculation indicates that 2-pyridyl is η^2-bonded to the Cp′$_2$Ce fragment in which the Ce–C and Ce–N bond distances are nearly equal at 2.5 Å, as are the Ce–N–C and Ce–C–N angles of ≈74° (Figure 9).
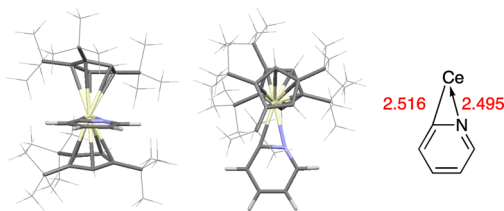
Figure 9. Top and side views of the optimized geometry of **1** with distances in Å.

The calculated structure of the trihydropyridyl complex **9** (Figure 10) gives a Ce–N bond distance of 2.381 Å, two Ce–N–C$_\alpha$(sp^3) and Ce–N–C$_\alpha$(sp^2) angles of 127 and 121°, respectively, and a torsion angle C$_t$–Ce–N–C$_\alpha$(sp^2) of 46°. The corresponding values in the solid-state structure are 2.327(3) Å for the Ce–N bond distance, 138.6(6)° for the Ce–N–C$_\alpha$(sp^3) angle, 104.3(2)° for the Ce–N–C$_\alpha$(sp^2) angle, and 73° for the average C$_t$–Ce–N–C$_\alpha$(sp^2) torsion angle. The calculated structure has a Ce–N bond distance too long by 0.05 Å and does not reproduce the Ce–N–C angles or the orientation of the trihydropyridyl ligand in the wedge of the Cp′$_2$Ce fragment.
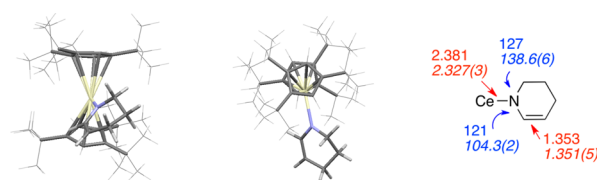
Figure 10. Top and side views of the optimized geometry of **9**, with distances in Å (red) and angles in degrees (blue). Experimental values are shown in italics.

In the piperidyl complex **13**, the calculated Ce–N bond distance is 2.346 Å and the two Ce–N–C$_\alpha$ angles are 124 and 126° (Figure 11). The NC$_5$H$_{10}$ ring has a chair conformation
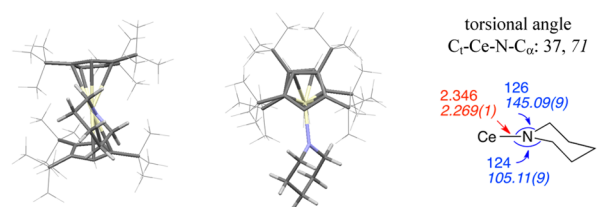
Figure 11. Top and side views of the optimized geometry of **13**, with distances in Å (red) and angles in degrees (blue). Experimental values are shown in italics.

with an average torsion angle C$_t$–Ce–N–C$_\alpha$ of 37°. These values do not agree with the solid-state structure. The experimental Ce–N bond distance is 2.269(1) Å, and the Ce–N–C$_\alpha$ and Ce–N–C$_{\alpha'}$ angles are 105.11(9)° and 145.09(9)°, respectively. The NC$_5$H$_{10}$ ring has a chair conformation, but the torsion angle C$_t$–Ce–N–C$_\alpha$ determined from the solid-state structure is 71°. Thus, the orientation of the piperidyl ring in the wedge of the Cp′$_2$Ce fragment is again not properly reproduced in the calculated structure.

The discrepancies between the calculated and experimental structures for **9** and **13** are similar, and they are associated with the position of the amide ligand in the wedge of the Cp′$_2$Ce fragment; that is, the Ce–N bond distances are too long, and the asymmetric orientation of the amide ligand is not properly reproduced. The influence of the level of calculations was tested on the piperidyl complex **13** without leading to any noticeable influence (see the SI). Moellmann and Grimme have recently shown that discrepancies between the calculated gas-phase and solid-state structures determined from X-ray crystallography can be resolved by consideration of the crystalline environment.[59] A simulation of the crystal packing (see the SI) gave results in close agreement with the solid-state stucture of **13**.[60] This rationalizes well the solid-state structure but still does not account for the solution ^{1}H NMR spectra, which are in accordance with the crystal structure.

The structures of the extrema for the reactions described in this work present no unusual features. As examples, the geometries of **3**–**5**, the reactant, transition state, and product, respectively, for the intramolecular hydrogen transfer from cerium to the α-carbon of pyridine and **Ce$_2$-6**, the transition state for the addition of [**Ce**]′-**H** to **5**, are discussed in the SI.

■ DISCUSSION

Hydrogenation of pyridine to piperidine is an exothermic reaction, $\Delta H = -47.5$ kcal mol^{-1}.[4] The reaction requires a catalyst because the addition of hydrogen to an isolated C=C or C=N double bond is a high-activation-energy process. Hydrogenation of pyridine begins with an equilibrium reaction

that forms the 2-pyridyl complex **1** (eq 6) and ends with the formation of **13**.

(6)
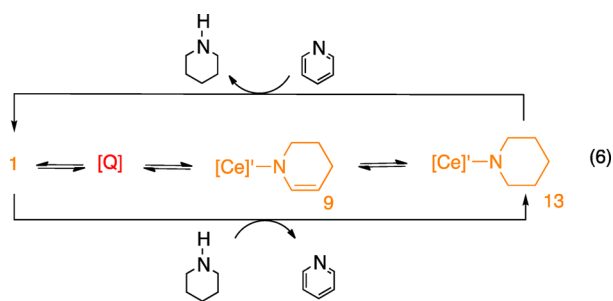
One intermediate, **9**, is observed when the reaction is monitored by changes in the ^{1}H NMR spectrum as a function of time. The reaction rate depends on the partial pressure of H_2 and on the presence of Cp'_2CeH, which is either deliberately added or formed by hydrogenolysis of the metal−carbon bonds formed along the reaction path. The calculated change in the Gibbs energy for the first hydrogen addition is endoergic, to form [Q] (eq 6), $\Delta G = +6$ kcal mol^{-1}, relative to separated reactants, but the next two additions are exoergic, −15.5 and −27.3 kcal mol^{-1}, respectively. The calculated values are in accordance with the experimental results that [Q] is not observed spectroscopically but both **9** and **13** are observed and isolated (eq 6). The addition of pyridine to **13**, which completes the cycle, is an equilibrium reaction in which the calculated change in the Gibbs energy is 2.2 kcal mol^{-1}.

A postulated mechanism for the hydrogenation reaction is developed from the experimental studies and the known reactivity patterns of Cp'_2CeH. Experimentally, the addition of pyridine to either Cp'_2CeH or $Cp'_2Ce(\eta^2\text{-}CH_2Ph)$ yields **1**. The first hydrogen addition occurs across the Ce−C(ortho) bond, followed by hydride transfer and rearrangement of the double bonds, forming [Q] postulated to be $Cp'_2Ce(6\text{-}$hydropyridyl). The addition of H_2 to Ce−C bonds, hydrogenolysis, is a well-known reaction in compounds of the general type Cp'_2CeR, where R is a hydrocarbyl.[36,52,54,61] The second step involves the addition of Cp'_2CeH across the γ,δ C=C double bond, followed by hydrogenolysis, affording **9**. The addition of Cp'_2CeH to olefins, such as cyclohexene, followed by hydrogenolysis, forming Cp'_2CeH and cyclohexane, is also a well-known reaction of Cp'_2CeH.[62] These two steps therefore involve conversion of the X−L ligand into an X ligand within the coordination sphere of Cp'_2Ce. The third step involves hydrogen addition to the remaining double bond, whose reaction rate is significantly slower than the first two additions, which is why **9**, but not [Q], is observed spectroscopically. The final step in the cycle is a proton transfer that regenerates **1**.

Experimentally, the rate of conversion of **1** to **9** is faster when a small amount of Cp'_2CeH, ca. 5 mol %, is deliberately added to **1** and H_2 or when the H_2 partial pressure is increased to 12 atm in the present study. However, the rate of conversion of **9** to **13** does not significantly depend on the presence of added Cp'_2CeH. Two possible reasons may be advanced for rate enhancement: (i) the kinetic rate law involves a pressure-dependent term in either the first or the second step, and (ii) if Cp'_2CeH appears in the experimental rate law, hydrogenolysis of any of the Ce−C bonds that form along the reaction coordinate increases its concentration and therefore the rate.

These three general steps are offered as postulates based on the qualitative experimental studies. A DFT computation study develops a more complete understanding of the transition states along the reaction coordinate.

Early modeling of the reactions of Cp'_2CeH with CH_3X (X = halide or OR),[36,62] and C_6F_6[51] used C_5H_5 as a model for Cp'. This modeling is not appropriate in the present case. For instance, the calculations with this modeling suggest that hydrogenation is easier at the carbon para to the nitrogen; details are available in the SI. Because this reaction is calculated to be reversible, isotope enrichment at the para carbon is expected but no detectable deuterium is observed in the para site in the experiment. Hydride addition to pyridine with Cp^*_2YH occurs at both of the ortho and para carbon atoms in pyridine,[32] in contrast to the reaction with Cp'_2CeH reported here. Consequently, the steric effects associated with the Me_3C groups on the rings control the regioselectivity of the hydride addition, and they are essential for modeling of the reaction path.

With the Cp'_2Ce model, the first hydride adds preferably at the carbon ortho to the nitrogen. The second hydrogen is introduced either by the heterolytic cleavage of H_2 or by the addition of Cp'_2CeH. In the two cases, a hydrogen atom is added to the carbon attached to the sp^3 carbon. The addition of Cp'_2CeH to a C=C double bond of **5** has a low-energy transition state, similar to that calculated for the addition of Cp'_2CeH to the double bond in cyclohexane, in agreement with the experiment. The addition of Cp'_2CeH to the C=C double bond is followed by hydrogenolysis of the resulting Ce−C bond of **Ce$_2$-7**, affording **9**. This accounts for the rate enhancement of added Cp'_2CeH. The high energy of the heterolytic addition of H_2 to **5** is associated with the unlikely orientation of the amido ligand required for H_2 to interact with the Cp'_2Ce fragment and the carbon of the amido ligand at the transition state.

■ CONCLUSION AND PERSPECTIVE

The combined experimental and computational study of the mechanism of hydrogenation of pyridine by Cp'_2CeH shows that the following reactions are involved. The pyridine adduct of Cp'_2CeH is not observed spectroscopically because it eliminates H_2, forming isolable **1**. The addition of H_2 to the latter, followed by hydride migration to the α-carbon, forms $Cp'_2Ce(6\text{-}$hydropyridyl). The addition of H_2 across the Ce−C σ bond in **1** is a heterolytic cleavage with a relatively high activation energy of 20 kcal mol^{-1}, but the activation energy for the hydride migration is only 12 kcal mol^{-1}, and these two steps are reversible. The addition of the second H_2 is the key reaction that begins the productive hydrogenation; this step involves the addition of Cp'_2CeH to the remote C=C double bond of $Cp'_2Ce(6\text{-}$hydropyridyl), which is followed by hydrogenolysis of the resulting Ce−C σ bond, regenerating Cp'_2CeH. These steps, which are associated with activation energies of less than 10 kcal mol^{-1}, lead to $Cp'_2Ce(4,5,6\text{-}$trihydropyridyl), an isolated intermediate. This step involves two Cp'_2Ce fragments, one of which is bound to the amide fragment and the other, present as Cp'_2CeH, hydrogenates the C=C double bond and is subsequently regenerated in the hydrogenolysis step. Therefore, Cp'_2CeH is a catalyst whose concentration accounts for the rate dependence on the partial pressure of H_2. The third H_2 addition across the C=N double bond is a repetition of these steps that proceed with somewhat higher activation energies. The key concept that emerges from this study is that

the mechanism requires intra- and intermolecular steps, which involve one and two Cp'_2Ce groups, respectively, and the intermolecular step is key for productive hydrogenation of pyridine because it is not reversible when H_2 is present.

The mechanisms discovered in the computational study of hydrogenation of pyridine are likely to be general for those metal compounds that do not undergo reductive elimination/oxidative addition reactions. An extension of the mechanistic patterns to hydrogenation of arenes, using benzene as an example, is apparent because the thermochemistry for conversion of benzene to cyclohexane is remarkably similar to that of pyridine (eq 7).[4]

$$C_6H_{6(g)} + 3H_{2(g)} \rightleftharpoons C_6H_{12(g)} \qquad \Delta H = -49 \text{ kcal mol}^{-1}$$

$$(7)$$
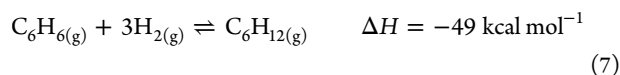
Benzene-d_6, however, is an inert solvent for the reactions in this and related reactions of Cp'_2CeH with CH_3X (X = halide, OR), and no reduction of benzene is observed. The metallacycle, in contrast, undergoes hydrogen for deuterium exchange in the Me_3C groups in C_6D_6, when H_2 is absent.[51] Even though hydrogenation of pyridine and benzene involve the addition of H_2 to C=C/N bonds, the rate of hydrogenation of benzene is clearly slower, presumably because of the high activation energy for the first addition of Cp'_2CeH to a C=C double bond of benzene due to the endothermicity of coordination. If bonding of an arene to the hydride complex were less endothermic, homogeneous hydrogenation of arenes should be possible.

The experimental results outlined in this manuscript were obtained several years ago. The computational results using C_5H_5 as a substitute for $1,2,4-(Me_3C)_3C_5H_2$ gave results in contradiction with the experimental ones, and calculations with the full ligands were not possible. Specifically, the size and conformational ambiguity of the full system prevented a complete exploration of the potential energy surfaces, which was the case with one Cp'_2CeH molecule; two were inconceivable. Today, this is not true because of the dramatic advances in computational power, and this long-standing problem waited patiently for the necessary computational advances. The reactivity studies and associated mechanistic questions outlined in this Forum Article, originated when the two senior authors were speakers at the Spanish Organometallic group meeting in Valladolid, Spain, in 2000.

ASSOCIATED CONTENT

Ⓢ Supporting Information

Crystal data for $Cp'_2Ce(NC_5H_8)$ (CCDC 955633) and $Cp'_2Ce(NC_5H_{10})$ (CCDC 955633), NMR plots (δ vs T^{-1}) for $Cp'_2Ce(NC_5H_{10})$, $Cp'_2Ce(NC_5D_{10})$, and $Cp'_2Ce(NC_5H_8)$, detailed energy profiles associated with Figures 6–8, calculations with the $(C_5H_5)_2Ce$ model, selected bond distances (Å) and angles (deg) at C(35) and C(39) in the piperidyl ligand of $[1,2,4-(Me_3C)_3C_5H_2]_2Ce(NC_5H_{10})$, calculations of the trihydropyridyl and piperidyl complexes, including the modeling of the crystal environment, presentation of the calculated structures of selected extrema (**3**, **4**, **5**, and **Ce$_2$-6**) on the reaction pathway, full experimental and computational details with associated references, and list of coordinates of all extrema with E, H, G, and dispersion contributions in atomic units. This material is available free of charge via the Internet at http://pubs.acs.org.

AUTHOR INFORMATION

Corresponding Authors
*E-mail: lionel.perrin@univ-lyon1.fr.
*E-mail: odile.eisenstein@univ-montp2.fr.
*E-mail: raandersen@lbl.gov.

Present Address
‡L.P.: Université Lyon 1, CNRS UMR 5246, Institut de Chimie et Biochimie Moléculaires et Supramoléculaires, 43 Boulevard du 11 Novembre 1918, F-69622 Villeurbanne, France.

Notes
The authors declare no competing financial interest.

REFERENCES

(1) Sánchez-Delgado, R. A. *Organometallic modeling of the hydrodesulfurization and hydrodenitrogenation reactions*; Kluwer Academic Publishers: Dordrecht, The Netherlands, 2002.

(2) Toshiaki, K.; Atsushi, I.; Weihua, Q. *Hydrodesulfurization and hydrodenitrogenation: chemistry and engineering*; Wiley-VCH: Tokyo, 1999.

(3) Crabtree, R. H. *Energy Environ. Sci.* **2008**, *1*, 134−138.

(4) (a) Ali, S. A. In *Hydroprocessing of Heavy Oils and Residua*; Speight, J. G., Ancheyta, J., Eds.; CRC Press: Boca Raton, FL, 2007; Chapter 4. (b) The black values are from ref 4a; the red values were extracted from: Cocchetto, J. F.; Satterfield, C. N. *Ind. Eng. Chem., Process. Des. Dev.* **1976**, *15*, 272−277 . The blue values are computed at the MO6-2X DFT level (see the SI).

(5) Rahi, R.; Fang, M.; Ahmed, A.; Sánchez-Delgado, R. A. *Dalton Trans.* **2012**, *41*, 14490−14497.

(6) Girgis, M. J.; Gates, B. C. *Ind. Eng. Chem. Res.* **1991**, *30*, 2021−2058.

(7) Busca, G. *Chem. Rev.* **2007**, *107*, 5366−5410.

(8) Glorius, F. *Org. Biomol. Chem.* **2005**, *3*, 4171−4175.

(9) Wang, D.-S.; Chen, Q.-A.; Lu, S.-M.; Zhou, Y.-G. *Chem. Rev.* **2012**, *112*, 2557−2590.

(10) Yu, Z.; Jin, W.; Jiang, Q. *Angew. Chem., Int. Ed.* **2012**, *51*, 6060−6072.

(11) Sonnemans, J.; Van den Berg, G. H.; Mars, P. *J. Catal.* **1973**, *31*, 220−230.

(12) Kliewer, C. J.; Somorjai, G. A. *Catal. Lett.* **2010**, *137*, 118−122.

(13) Kliewer, C. J.; Bieri, M.; Somorjai, G. A. *J. Phys. Chem. C* **2008**, *112*, 11373−11378.

(14) Li, Y.; Guo, W.; Zhu, H.; Zhao, L.; Li, M.; Li, S.; Fu, D.; Lu, X.; Shan, H. *Langmuir* **2012**, *28*, 3129−3137.

(15) Weller, K. J.; Fox, P. A.; Gray, S. D.; Wigley, D. E. *Polyhedron* **1997**, *16*, 3139−3163.

(16) Bianchini, C.; Meli, A.; Vizza, F. *Eur. J. Inorg. Chem.* **2001**, 43−68.

(17) Dobereiner, G.; Nova, A.; Schley, N.; Hazari, N.; Miller, S.; Eisenstein, O.; Crabtree, R. H. *J. Am. Chem. Soc.* **2011**, *133*, 7547−7562.

(18) Sánchez-Delgado, R. A.; Ronden, D.; Andriollo, A.; Herrera, V.; Martin, G.; Chaudret, B. *Organometallics* **1993**, *12*, 4291−4296.

(19) Rosales, M.; Vallejo, R.; Soto, J. J.; Bastidas, L. J.; Molina, K.; Baricelli, P. *J. Catal. Lett.* **2010**, *134*, S6−62.

(20) Rosales, M.; Alvarado, Y.; Boves, M.; Rubio, R.; Soscun, H.; Sánchez-Delgado, R. A. *Transition Met. Chem.* **1995**, *20*, 246−251.

(21) Bianchini, C.; Barbaro, P.; Macchi, M.; Meli, A.; Vizza, F. *Helv. Chim. Acta* **2001**, *84*, 2895−2932.

(22) Magee, M. P.; Norton, J. R. *J. Am. Chem. Soc.* **2001**, *123*, 1778−1779.

(23) Bullock, R. M. *Chem.—Eur. J.* **2004**, *10*, 2366−2374.

(24) Guan, H.; Iimura, M.; Magee, M. P.; Norton, J. R.; Zhu, G. *J. Am. Chem. Soc.* **2005**, *127*, 7805−7814.

(25) Zhou, H.; Li, Z.; Wang, Z.; Wang, T.; Xu, L.; He, Y.; Fan, Q.-H.; Pan, J.; Gu, L.; Chan, A. S. C. *Angew. Chem., Int. Ed.* **2008**, *47*, 8464−8467.

(26) Eisenstein, O.; Crabtree, R. H. *New J. Chem.* **2013**, *37*, 21−27.

(27) Jardine, I.; McQuillin, F. J. *J. Chem. Soc., Chem. Commun.* **1970**, 626.

(28) Baralt, E.; Smith, S. J.; Hurwitz, J.; Horvath, I. T.; Fish, R. H. *J. Am. Chem. Soc.* **1992**, *114*, 5187−5196.

(29) Borowski, A. F.; Sabo-Etienne, S.; Donnadieu, B.; Chaudret, B. *Organometallics* **2003**, *22*, 4803−4809.

(30) Berno, P.; Gambarotta, S. *Organometallics* **1994**, *13*, 2569−2571.

(31) Watson, P. L. *J. Chem. Soc., Chem. Commun.* **1983**, 276−277.

(32) Deelman, B.-J.; Stevels, W. M.; Teuben, J. H.; Lakin, M. T.; Spek, A. L. *Organometallics* **1994**, *13*, 3881−3891.

(33) Thompson, M. E.; Baxter, S. M.; Bulls, A. R.; Burger, B. J.; Nolan, M. C.; Santarsiero, B. D.; Schaefer, W. P.; Bercaw, J. E. *J. Am. Chem. Soc.* **1987**, *109*, 203−219.

(34) Evans, W. J.; Hughes, L. A.; Hanusa, T. P. *J. Am. Chem. Soc.* **1984**, *106*, 4270−4271.

(35) Diaconescu, P. L. *Curr. Org. Chem.* **2008**, *12*, 1388−1405.

(36) Werkema, E. L.; Andersen, R. A.; Yahia, A.; Maron, L.; Eisenstein, O. *Organometallics* **2009**, *28*, 3173−3185.

(37) Booth, H.; Everett, J. R. *J. Chem. Soc., Chem. Commun.* **1979**, 34−35.

(38) Heeres, H. J.; Meetsma, A.; Teuben, J. H.; Rogers, R. D. *Organometallics* **1989**, *8*, 2637−2646.

(39) Hitchcock, P. B.; Lappert, M. F.; Protchenko, A. V. *Chem. Commun.* **2006**, 3546−3548.

(40) Fjeldberg, T.; Andersen, R. A. *J. Mol. Struct.* **1985**, *129*, 93−105.

(41) Werkema, E. L.; Andersen, R. A.; Maron, L.; Eisenstein, O. *Dalton Trans.* **2010**, *39*, 6648−6660.

(42) Gundersen, G.; Rankin, D. W. H. *Acta Chem. Scand., Ser. A* **1983**, *37*, 865−874.

(43) Brookhart, M.; Green, M. L. H. *J. Organomet. Chem.* **1983**, *250*, 395−408.

(44) Brookhart, M.; Green, M. L. H.; Wong, L. L. *Prog. Inorg. Chem.* **1988**, *36*, 1−124.

(45) Brookhart, M.; Green, M. L. H.; Parkin, G. *Proc. Natl. Acad. Sci. U.S.A.* **2007**, *104*, 6908−6914.

(46) Clot, E.; Eisenstein, O. In *Principles and Applications of Density Functional Theory in Inorganic Chemistry II*; Kaltsoyannis, N., McGrady, J. E., Eds.; Structure and Bonding Series; Springer-Verlag: Heidelberg, Germany, 2004; Vol. *113*, pp 1−36.

(47) Balcells, D.; Clot, E.; Eisenstein, O. *Chem. Rev.* **2010**, *110*, 749−823.

(48) Scherer, W.; Herz, V.; Hauf, C. *Structure and Bonding (Berlin)*; Springer-Verlag: Heidelberg, Germany, 2012; Vol. *146*, pp 159−208.

(49) Lein, M. *Coord. Chem. Rev.* **2009**, *253*, 625−634.

(50) Pauling, L. *The Nature of the Chemical Bond*, 3rd ed.; Cornell University Press: Ithaca, NY, 1960.

(51) Maron, L.; Werkema, E. L.; Perrin, L.; Eisenstein, O.; Andersen, R. A. *J. Am. Chem. Soc.* **2005**, *127*, 279−292.

(52) Werkema, E. L.; Maron, L.; Eisenstein, O.; Andersen, R. A. *J. Am. Chem. Soc.* **2007**, *129*, 2529−2541 (correction on p 6662).

(53) Werkema, E. L.; Yahia, A.; Maron, L.; Eisenstein, O.; Andersen, R. A. *Organometallics* **2010**, *29*, 5103−5110.

(54) Werkema, E. L.; Castro, L.; Maron, L.; Eisenstein, O.; Andersen, R. A. *Organometallics* **2012**, *31*, 870−881.

(55) Werkema, E. L.; Castro, L.; Maron, L.; Eisenstein, O.; Andersen, R. A. *New J. Chem.* **2013**, *37*, 132−142.

(56) Schafman, B. S.; Wenthold, P. G. *J. Org. Chem.* **2007**, *72*, 1645−1651.

(57) Wren, S. W.; Vogelhuber, K. M.; Garver, J. M.; Kato, S.; Sheps, L.; Bierbaum, M.; Lineberger, W. C. *J. Am. Chem. Soc.* **2012**, *134*, 6584−6595.

(58) As noted in footnote 22 in ref 22, cyclohexene reacts rapidly with Cp'_2CeH, generating the cyclohexyl derivative that yields the metallacycle and cyclohexane. Under H_2, the metallacycle or Cp'_2CeH is a hydrogenation catalyst for cyclohexene.

(59) Moellmann, J.; Grimme, S. *Organometallics* **2013**, *32*, 3784−3787.

(60) A periodic approach is under study and will be presented in a separate article.

(61) Werkema, E. L.; Yahia, A.; Maron, L.; Eisenstein, O.; Andersen, R. A. *New J. Chem.* **2010**, *34*, 2189−2196.

(62) Werkema, E. L.; Messines, E.; Perrin, L.; Maron, L.; Eisenstein, O.; Andersen, R. A. *J. Am. Chem. Soc.* **2005**, *127*, 7781−7795.

6373

dx.doi.org/10.1021/ic500133y | *Inorg. Chem.* 2014, 53, 6361−6373